Research Article | Vol. 28, No. 8 / 13 April 2020 / Optics Express 12037
Optics EXPRESS

Switching the second harmonic generation by a dielectric metasurface via tunable liquid crystal

DAVIDE ROCCO,[1,2,*] LUCA CARLETTI,[1,3] ROBERTO CAPUTO,[4,5] MARCO FINAZZI,[6] MICHELE CELEBRANO,[6] AND COSTANTINO DE ANGELIS[1,2]

[1]Department of Information Engineering, University of Brescia, via Branze 38, Brescia 25123, Italy
[2]National Institute of Optics (INO), via Branze 45, 25123 Brescia, Italy
[3]Department of Information Engineering, University of Padova, via G. Gradenigo 6/B, Padova, Italy
[4]Department of Physics & CNR-NANOTEC, University of Calabria, via P. Bucci, Cubo 31 C, Rende 87036, Italy
[5]Institute of Fundamental and Frontier Sciences, University of Electronic Science and Technology of China, Chengdu 610054, China
[6]Department of Physics, Politecnico di Milano, Piazza Leonardo Da Vinci 32, Milano 20133, Italy
[*]d.rocco003@unibs.it

Abstract: Optical modulators are key ingredients in optoelectronics applications ranging from energy harvesting, sensor and imaging devices. In this framework, nonlinear photon conversion mechanisms constitute an attractive opportunity to add logic capabilities to these apparatuses. Here, we investigate the directionality of the emitted second harmonic signal generated in a dielectric metasurface consisting of AlGaAs nanocylinders embedded into a liquid crystal matrix. We numerically demonstrate that, by switching the liquid crystal orientation with a realistic voltage bias, it is possible to modulate the total power and the emission pattern of the SH signal coming from the proposed metasurface. Our results open important opportunities for tunable metadevices such as nonlinear holograms and dynamic displays.

1. Introduction

High refractive index dielectric and semiconductors nanostructures emerged as excellent candidates for nanophotonic applications. The possibility to tune their radiation profiles or the ability to control the polarization of the scattered light with very low losses with respect to metallic nanodevices, in the near-infrared and visible region of the electromagnetic spectrum, have drawn considerable attention to the photonic research field [1–5]. In this regard, semiconductors are attractive materials due to their high permittivity and the ability to tune their optical properties by varying the geometrical aspect ratio or the carrier density through appropriate doping.

The resonant enhancement of the fields inside semiconductor resonators has been already demonstrated to boost nonlinear frequency generation [6–8]. Silicon, the most technically relevant semiconductor, would be the natural choice for microelectronic compatibility [9]. However, silicon is not suitable for even-order nonlinear bulk processes due to its centro-symmetric crystal structure. Physically, when silicon is excited, the even-order nonlinear susceptibility tensors are strictly equal to zero, thus making even-order nonlinear processes forbidden. In contrast, odd-order nonlinear processes are always allowed [10,11]. On the other hand, III-V semiconductors such as Gallium Arsenide, GaAs, or Aluminum Gallium Arsenide, AlGaAs display remarkably high even-order susceptibilities thanks to the broken central symmetry in their crystal structure [12,13]. In particular, AlGaAs exhibits a direct gap which increases with the Aluminum molar fraction, enabling Two Photons Absorption (TPA) free operation at 1550 nm. As a result, efficient SH generation (SHG) from nanostructured AlGaAs was recently demonstrated in different scenarios, either in isolated nanoantennas or in metasurfaces [14–16].

#386776 https://doi.org/10.1364/OE.386776
Journal © 2020 Received 26 Dec 2019; revised 28 Jan 2020; accepted 28 Jan 2020; published 8 Apr 2020

Optics EXPRESS

In many practical applications, it is crucial to enable dynamic tunability of the device behavior. A possible solution for the realization of tunable devices is offered by anisotropic materials [17–21]. In this context, the use of Liquid Crystals (LCs) is an attractive approach because it relies on the well-established expertise from the LC display industry [22,23]. LCs have an optical birefringence that can be tuned by applying an external electric field or by increasing the working temperature. Recently, it has been demonstrated that the spectral positions of the Mie resonances of a silicon metasurface can be tuned by employing an external electric field that reorients the surrounding nematic liquid crystal, thus achieving a transmission modulation [24]. Also, a switchable beam deflection metadevice has been proposed in a silicon-nanodisk dielectric metasurface infiltrated with liquid crystals, which relies on heating the metasurface to modify the LC state and thus the direction of the scattered light beam [25]. However, the control and optimization of the nonlinear response of the scattered harmonic light in such metasurfaces remain a major challenge.

Here, we propose, for the first time to our knowledge, a design based on a semiconductor metasurface made of AlGaAs nanodisks on an AlOx substrate embedded in a nematic LC matrix (Merck Licristal E7). The LC high birefringence (~0.2) at room temperature allows us to finely control the Front-to-Back Ratio (FBR) of the SH signal of the metasurface and to achieve a directional modulation of the SH emission. We thus theoretically demonstrate a 10-fold enhancement in the FBR of the SH signal for a fixed incident wavelength for the two different LC states (planar and homeotropic alignments). We achieve this result by calculating the variation of the second harmonic signal for two extremal cases, corresponding to a LC director aligned either parallel or perpendicular to the metasurface plane. The obtained results pave the way for the realization of dynamically tunable nonlinear metasurfaces with numerous applications including nonlinear holography, imaging and active beam shaping.

2. Result and discussion

We consider a metasurface composed of AlGaAs nanodisks on top of an AlOx substrate embedded into an LC cell, as schematically sketched in Fig. 1. In our calculations we assume nanocylinders with a height h of 200 nm and a radius r of 280 nm with the AlGaAs zincblende 100 crystallographic directions aligned parallel to the laboratory cartesian axes, as indicated

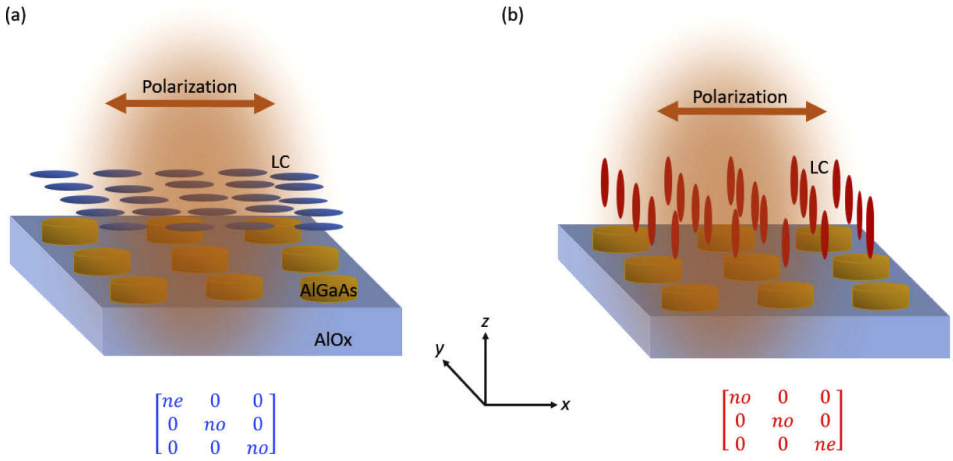

Fig. 1. Sketch of the proposed metasurface in the case of (a) initial LC director parallel to the x axis (planar alignment) and (b) LC directions in the vertical orientation (homeotropic alignment). The orange arrow represents the fixed incident light polarization.

Optics EXPRESS

in Fig. 1. The period of the metasurface is 909 nm. These dimensions are selected such that the electric and magnetic dipolar resonances are excited in the third communication window range. Moreover, the chosen geometrical parameters guarantee the maximum variation of the SH emission pattern upon realignment of the LC (see Appendix, Fig. 5). The AlOx layer is assumed to be semi-infinite extending along the z-axis with a refractive index equal to 1.6 [6]. The dispersion of AlGaAs is taken from [8]. We consider the E7 nematic LC (Merck Licristal) that is a widely used liquid crystal for applications in displays and we analyze two cases (configurations). The first one is for the initial LC director (the optical axis) parallel to the x axis [planar alignment, Fig. 1(a)], corresponding to the unbiased state with n_x=n_e=, n_y=n_o, n_z=n_o, where n_o and n_e are the refractive indices along the ordinary and extraordinary axes; the other is the extreme situation where the LC director is vertically oriented [e.g. along z, homeotropic alignment, Fig. 1(b)] with n_x=n_o, n_y=n_o, n_z=n_e. The excitation is assumed to be a plane wave normally incident on the AlGaAs nanoantenna substrate with the electric field E_0 polarized in the x direction and an intensity of 1GW/cm^2.

We use COMSOL Multiphysics to estimate the scattering behavior of the proposed structure. The LC is simulated as a homogeneous anisotropic dielectric medium with n_e=1.703 and n_0=1.502 for the fundamental wavelength region (1400 nm - 1800nm) and n_e=1.7209, n_0=1.512 for the SH wavelengths (700 nm - 900 nm) assuming a working temperature of 20 °C [26], corresponding to the values observed in a typical E7 LC (produced by Merck) [27,28]. In considering a homogeneous LC layer for the two configurations we implicitly neglect possible effects due to a stable anchoring of the LC molecules to the nanostructures, a phenomenon that reduces the LC anisotropy [29]. Therefore, our calculations describe a best-case scenario in which the variation of the nonlinear optical properties of the metasurface between the two configurations is maximized, which may serve as a benchmark for possible real-world devices. Figure 2 summarizes the transmittance obtained for the two considered cases. As it has been already reported, the anisotropy of the LC introduces a shift and a modification in the scattering properties of the metasurface [24]. To gain a deeper physical insight in the behavior of the metasurface, the optical response is expanded using a spherical multipole decomposition via integration of the induced currents inside the AlGaAs resonators [30]. Although the numerical simulations take into account the presence of the substrate and the anisotropy of the liquid crystal above the disks, the multipoles are simply calculated as if they were radiating into a homogenous medium with refractive index respectively equal to n_e and n_0 for the LC director being respectively parallel or orthogonal to the x axis. Despite this rough approximation, the found multipoles are in good agreement with the numerical linear scattering [see Figs. 2(b) and 2(c)]. A further confirmation of the qualitative soundness of this approach is provided by the observation of the electric field distribution maps inside the dielectric nanodisks, which confirms the dipolar electric or magnetic nature of the mode for the same wavelengths (see Appendix, Fig. 6), as indicated by the multipolar decomposition. More precisely, the ED resonance is excited at 1496 nm and around 1630 nm for the planarly aligned LC and at 1550 nm in the case of homeotropic LC alignment. Instead, the magnetic dipolar (MD) peak contribution undergoes a red shift from a wavelength of 1508 nm to a wavelength of 1580 nm after a full reorientation of the LC director along the z axis, see Fig. 2.

To study the SHG process we calculate the fields at the fundamental frequency to define the SH sources in terms of current densities. Due to the AlGaAs zincblende crystalline structure, the i-th component of the external current density J_i is calculated as: $J_i = \mathrm{j}\omega_{SH}\varepsilon_0\chi^{(2)}E_{FF,j}E_{FF,k}$ with $i\neq j\neq k$, where ε_0 is the vacuum permittivity, $E_{FF,i}$ is the i-th component of the electric field at the fundamental frequency and $\chi^{(2)}$ is the nonlinear second-order susceptibility, which we assume to be equal to 100 pm/V [6]. Only the high-refractive-index nanodisks have been considered as the harmonic source since the considered liquid crystal material and the AlOx substrate have both a negligible $\chi^{(2)}$ [6,31]. Figure 3 shows the total SH efficiency, calculated as the ratio

Optics EXPRESS

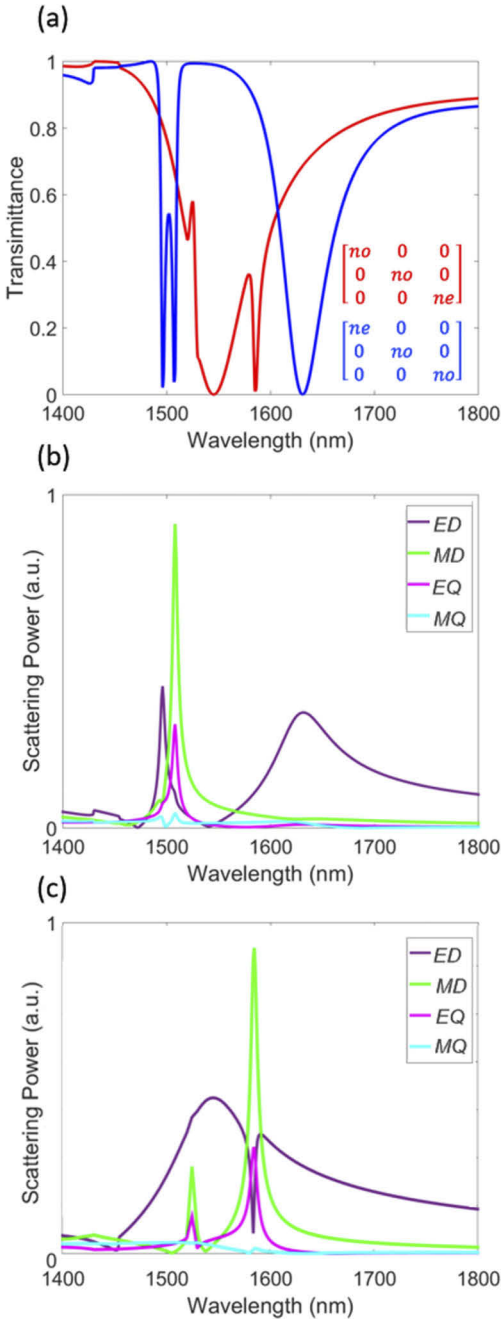

Fig. 2. (a) Numerical calculations of the spectral resonances for the two LC orientations: the blue curve refers to the LC directors parallel to the x axis while the red curve refers to the LC directors parallel to the z axis. Metasurface multipolar scattering decomposition for LC directors oriented parallel (b) or orthogonal (c) to the x axis. The coefficients *ED, MD, EQ* and *MQ* are associated to electric dipole, magnetic dipole, electric quadrupole, and magnetic quadrupole contributions, respectively.

Optics EXPRESS

between the total scattered SH power and the incident power on the unitary cell area, for the two different configurations of the LCs. The main SHG peak is due to the magnetic dipolar resonance for both cases: at 1508 nm when the LCs are in a planar alignment (blue line) and around 1580 nm when the LCs are in a homeotropic one (red one). Also the secondary peak of Fig. 3 (red curve) is mainly dominated by the MD contribution (see Fig. 6 in the Appendix for the exact field distribution at 1526 nm). In this way, for a fixed incident fundamental wavelength and polarization, we obtain a SH modulator that is activated by spectrally shifting the MD of the nanodisks 'on' and 'off' resonance by switching the liquid crystal orientation.

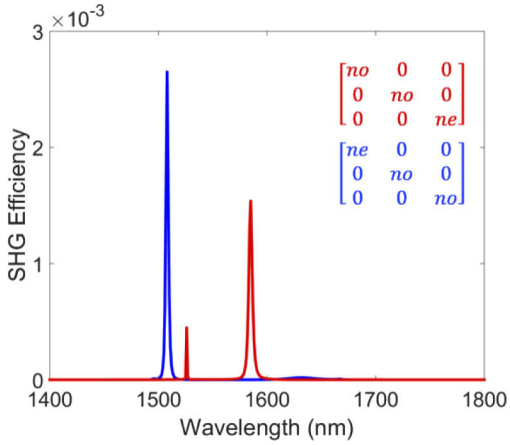

Fig. 3. Second harmonic efficiency as a function of the fundamental wavelength for LCs in a planar alignment (director parallel to the x axis, blue curve) and in a homeotropic one (director oriented along the z axis, red curve).

The total scattered power coming from the metasurface is not the only relevant parameter characterizing the nonlinear harmonic behavior. In fact, a crucial issue to deal with when using AlGaAs on AlOx platform is that the SH scattered power is mostly irradiated into the substrate region, which is the denser medium since the upper medium is usually air [6,32–33]. In the proposed metasurface, the upper medium is filled with a high index anisotropic liquid crystal with n_e higher than the refractive index of the AlOx substrate. This adds a degree of freedom in the system under investigation and opens the possibility of having a SH radiation that is not backscattered in the substrate but mainly radiated in the upper half space. For this reason, we study the FBR of the SH signal for the two different LC orientations. More precisely, the SH FBR is defined as the SH power scattered in the upper region divided by the SH power scattered in the lower region. This calculation is performed at a distance of $5\lambda_{\mathrm{SHG}}$ where λ_{SHG} is the SH wavelength, from the nanodisk in the LCs or in the substrate regions, respectively. It is evident from Fig. 4(a) that for the liquid crystal director in a homeotropic alignment (red curve) the FBR shows a maximum which is much larger than one (roughly 6.5) at 1576 nm, in the proximity of the SH generation peak due to the magnetic dipolar resonance excitation inside the nanodisk. For the same wavelength, the FBR for the other LC orientation (director oriented along x) reaches a value of 0.65. This demonstrates that the proposed structure is capable of modifying the FBR of the SH signal by changing the orientation of the LCs. Notably, for a fixed wavelength, an increase of one order of magnitude is obtained. We point out that maximizing the SH FBR is of paramount importance in reflection set-up geometries, which has to be adopted for thick or unpolished substrates. Furthermore, the proposed metasurface exhibits a 5-fold enhancement in the SH FBR when we compare the behavior of the two LCs orientations around the wavelengths of the respective magnetic resonances [see Figs. 3 and 4(a)]. Indeed, the absolute

Optics EXPRESS

maximum of the second harmonic FBR for the liquid crystals oriented along the x axis is reached at 1497 nm and it is less than 1.4. For completeness, Figs. 4(b) and (c) show the different second harmonic field distribution inside the cylinder respectively for the blue and for the red curve of Fig. 4(a), demonstrating that the different electric field of the second harmonic signal around the wavelengths of the magnetic dipolar resonance is responsible for the distinct behavior of the SH emission.

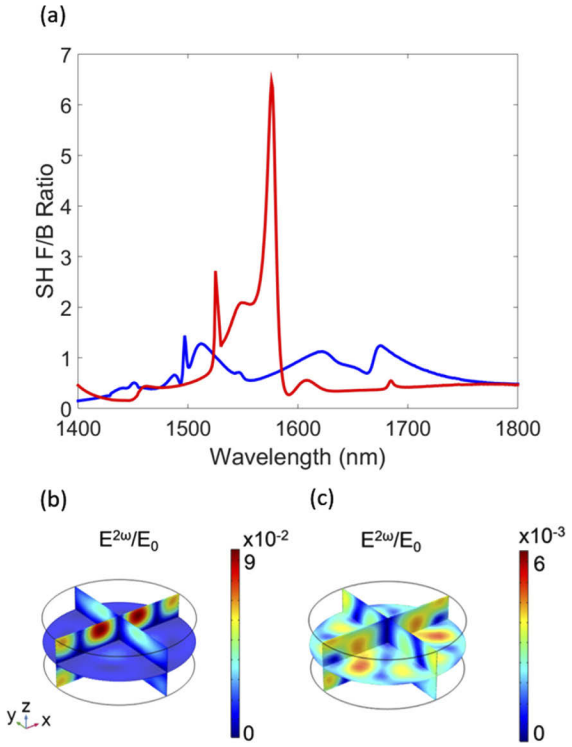

Fig. 4. (a) Numerical calculations of the second harmonic FBR as a function of the fundamental wavelength for the two LC orientations: the blue curve refers to the LC directors parallel to the x axis while the red curve refers to the LC directors parallel to the z axis. Second harmonic field distribution inside the AlGaAs cylinder of the metasurface (b) for an incident wavelength of 1497 nm for the LC oriented in the xy plane and (c) for an excitation wavelength of 1576 nm nm and LC aligned in the xz plane. The plots are normalized to the incident electric field E_0.

3. Conclusions

To conclude, we have demonstrated the possibility to obtain a nonlinear SH modulator by utilizing liquid crystals as the upper media of a dielectric metasurface. In fact, for a fixed wavelength, by switching between the two LC states (planar and homeotropic), the SH signal can be activated or turned off. Moreover, we have demonstrated that the LC anisotropy can be exploited to modulate the FBR of the SH emission coming from the optimized metastructure, demonstrating an enhancement of one order of magnitude in the nonlinear FBR for the two different liquid crystal states for the same incident wavelength and polarization of the excitation beam. Our predictions represent a step forward for the realization of dynamically tunable mateasurfaces, which might have several applications, including tunable imaging and active beam shaping.

Optics EXPRESS

Appendix

Calculation of the optimal parameters

Figure 5 represents the difference of the SH Front-to-Back ratio for the two different LC orientations as a function of the geometrical parameters of the metasurface for a fixed incident wavelength equal to1576 nm. In the article, we have selected the parameters that maximize the variation of the SH signal emission.

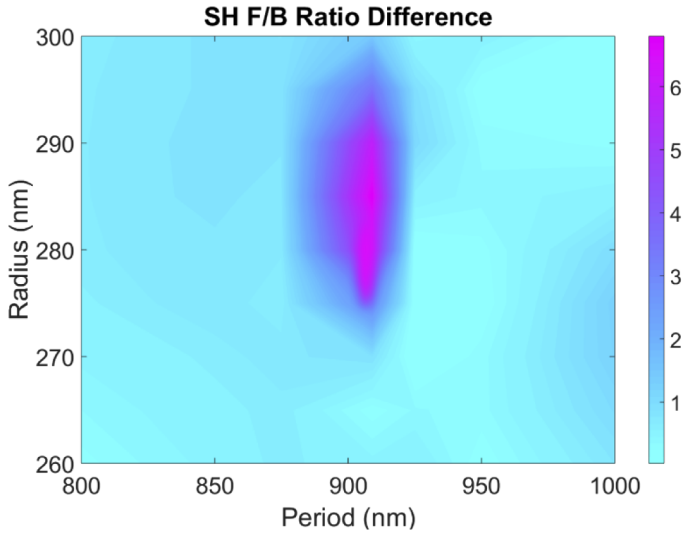

Fig. 5. SH Front-to-Back Ratio Difference as a function of the radius of tha AlGaAs nanodisks and the period of the metasurface. The incident signal is assumed to be a x-polarized plane wave at 1576 nm.

Electric field map at the multipolar resonances

Figure 6 shows the electric field distribution inside the AlGaAs nanocylinder that forms the metasurface at the wavelength of interest, see Fig. 2(a) for comparison. The nature of the excited multipoles is clearly distinguishable from the electric field map in Fig. 6. The MD resonance is characterized by an electric field loop [see Figs. 6(b), 6(d) and 6(f)], instead the ED one by the linearly polarized electric field in the nanoantenna volume [Figs. 6(a), 6(c) and 6(e)].

Optics EXPRESS

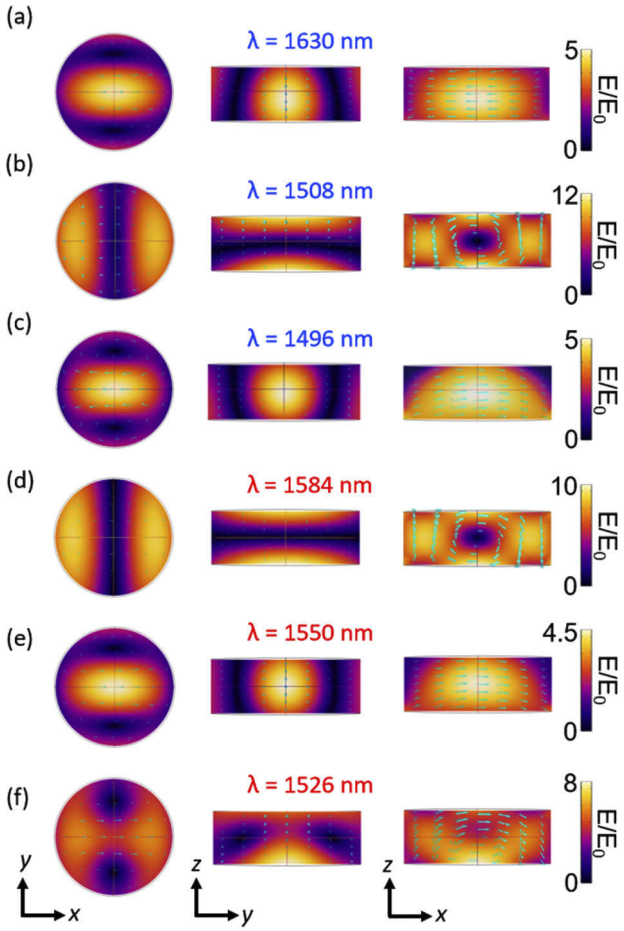

Fig. 6. (a), (b) and (c) show the electric field distribution map inside the dielectric nanodisk for a planar LC alignment and an incident wavelength equal to 1630 nm, 1508 nm and 1496 respectively. The electric field enhancement inside the resonator for the homeotropic LC orientation is plotted in (d), (e) and (f) for wavelengths equal to 1584 nm, 1550 nm and 1526 nm. The light blue arrows refer to the electric field vector.

Funding

Ministero dell'Istruzione, dell'Università e della Ricerca (2017MP7F8F); Consiglio Nazionale delle Ricerche (Joint Lab Project).

Disclosures

The authors declare no conflicts of interest.

References

1. A. E. Krasnok, A. E. Miroshnichenko, P. A. Belov, and Y. S. Kivshar, "All-dielectric optical nanoantennas," Opt. Express **20**(18), 20599–20604 (2012).
2. L. Zou, W. Withayachumnankul, C. M. Shah, A. Mitchell, M. Bhaskaran, S. Sriram, and C. Fumeaux, "Dielectric resonator nanoantennas at visible frequencies," Opt. Express **21**(1), 1344–1352 (2013).
3. D. S. Filonov, A. E. Krasnok, A. P. Slobozhanyuk, P. V. Kapitanova, E. A. Nenasheva, Y. S. Kivhar, and P. A. Belov, "Experimental verification of the concept of all-dielectric nanoantennas," Appl. Phys. Lett. **100**(20), 201113 (2012).

Optics EXPRESS

4. P. Albella, R. A. de la Osa, F. Moreno, and S. A. Maier, "Electric and magnetic field enhancement with ultralow heat radiation dielectric nanoantennas: considerations for surface-enhanced spectroscopies," ACS Photonics **1**(6), 524–529 (2014).
5. Y. Yang, W. Wang, A. Boulesbaa, I. I. Kravchenko, D. P. Briggs, A. Puretzky, and D. Geohegan, "Nonlinear Fano-resonant dielectric metasurfaces," Nano Lett. **15**(11), 7388–7393 (2015).
6. V. F. Gili, L. Carletti, A. Locatelli, D. Rocco, M. Finazzi, L. Ghirardini, I. Favero, C. Gomez, A. Lemaitre, M. Celebrano, C. De Angelis, and G. Leo, "Monolithic AlGaAs second-harmonic nanoantennas," Opt. Express **24**(14), 15965–15971 (2016).
7. V. F. Gili, L. Ghirardini, D. Rocco, G. Marino, I. Favero, I. Roland, G. Pellegrini, L. Duò, M. Finazzi, L. Carletti, A. Locatelli, A. Lemaitre, D. Neshev, C. De Angelis, G. Leo, and M. Celebrano, "Metal–dielectric hybrid nanoantennas for efficient frequency conversion at the anapole mode," Beilstein J. Nanotechnol. **9**, 2306–2314 (2018).
8. D. Rocco, V. F. Gili, L. Ghirardini, L. Carletti, I. Favero, A. Locatelli, G. Marino, D. N. Neshev, M. Celebrano, M. Finazzi, G. Leo, and C. De Angelis, "Tuning the second-harmonic generation in AlGaAs nanodimers via non-radiative state optimization," Photonics Res. **6**(5), B6–B12 (2018).
9. R. F. Wolffenbuttel, *Silicon sensors and circuits: on-chip compatibility*. Springer Science & Business Media (1996).
10. M. R. Shcherbakov, D. N. Neshev, B. Hopkins, A. S. Shorokhov, I. Staude, E. V. Melik-Gaykazyan, M. Decker, A. E. Ezhov, A. E. Miroshnichenko, I. Brener, A. A. Fedyanin, and Y. S. Kivshar, "Enhanced third-harmonic generation in silicon nanoparticles driven by magnetic response," Nano Lett. **14**(11), 6488–6492 (2014).
11. L. Xu, M. Rahmani, K. Z. Kamali, A. Lamprianidis, L. Ghirardini, J. Sautter, R. Camacho-Morales, H. Chen, M. Parry, I. Staude, G. Zhang, D. Neshev, and A. E. Miroshnichenko, "Boosting third-harmonic generation by a mirror-enhanced anapole resonator," Light: Sci. Appl. **7**(1), 44 (2018).
12. M. Timofeeva, A. Bouravleuv, G. Cirlin, I. Shtrom, I. Soshnikov, M. R. Escalé, A. Sergeyev, and R. Grange, "Polar second-harmonic imaging to resolve pure and mixed crystal phases along GaAs nanowires," Nano Lett. **16**(10), 6290–6297 (2016).
13. L. Carletti, A. Locatelli, O. Stepanenko, G. Leo, and C. De Angelis, "Enhanced second-harmonic generation from magnetic resonance in AlGaAs nanoantennas," Opt. Express **23**(20), 26544–26550 (2015).
14. R. Camacho-Morales, M. Rahmani, S. Kruk, L. Wang, L. Xu, D. A. Smirnova, A. S. Solntsev, A. Miroshnichenko, H. Hoe Tan, F. Karouta, S. Naureen, K. Vora, L. Carletti, C. De Angelis, C. Jagadish, Y. S. Kivshar, and D. N. Neshev, "Nonlinear generation of vector beams from AlGaAs nanoantennas," Nano Lett. **16**(11), 7191–7197 (2016).
15. L. Xu, M. Rahmani, D. Smirnova, K. Z. Kamali, G. Zhang, D. Neshev, and A. E. Miroshnichenko, "Highly-efficient longitudinal second-harmonic generation from doubly-resonant Algaas nanoantennas," Photonics **5**(3), 20 (2018).
16. P. P. Vabishchevich, S. Liu, M. B. Sinclair, G. A. Keeker, G. M. Peake, and I. Brener, "Enhanced second-harmonic generation using broken symmetry III–V semiconductor Fano metasurfaces," ACS Photonics **5**(5), 1685–1690 (2018).
17. E. Salahun, P. Queffelec, and G. Tanne, "Correlation between magnetic properties of layered ferromagnetic/dielectric material and tunable microwave device applications," J. Appl. Phys. **91**(8), 5449–5455 (2002).
18. C. Y. Liu and L. W. Chen, ". Tunable band gap in a photonic crystal modulated by a nematic liquid crystal," Phys. Rev. B **72**(4), 045133 (2005).
19. A. Locatelli, C. De Angelis, D. Modotto, S. Boscolo, F. Sacchetto, M. Midrio, A. D. Capobianco, F. M. Pigozzo, and C. G. Someda, "Modeling of enhanced field confinement and scattering by optical wire antennas," Opt. Express **17**(19), 16792–16800 (2009).
20. C. De Angelis, A. Locatelli, D. Modotto, S. Boscolo, M. Midrio, and A. D. Capobianco, "Frequency addressing of nano-objects by electrical tuning of optical antennas," J. Opt. Soc. Am. B **27**(5), 997–1001 (2010).
21. A. Minovich, J. Farnell, D. N. Neshev, I. McKerracher, and F. Karouta, "Liquid crystal based nonlinear fishnet metamaterials," Appl. Phys. Lett. **100**(12), 121113 (2012).
22. B. Splingart, N. Tentillier, F. Huret, and C. Legrand, "Liquid crystals applications to RF and microwave tunable components," Mol. Cryst. Liq. Cryst. Sci. Technol., Sect. A **368**(1), 183–190 (2001).
23. P. Yaghmaee, O. H. Karabey, B. Bates, C. Fumeaux, and R. Jakoby, "Electrically tuned microwave devices using liquid crystal technology," Int. J. Antenn. Propag. **2013**, 1–9 (2013).
24. A. Komar, Z. Fang, J. Bohn, J. Sautter, M. Decker, A. Miroshnichenko, T. Pertsch, I. Brener, Y. S. Kivshar, I. Staude, I. and D, and N. Neshev, "Electrically tunable all-dielectric optical metasurfaces based on liquid crystals," Appl. Phys. Lett. **110**(7), 071109 (2017).
25. A. Komar, R. Paniagua-Dominguez, A. Miroshnichenko, Y. Feng Yu, Y. Kivshar, A. I. Kuznetsov, and D. Neshev, "Dynamic beam switching by liquid crystal tunable dielectric metasurfaces," ACS Photonics **5**(5), 1742–1748 (2018).
26. J. Li, S. T. Wu, S. Brugioni, R. Meucci, and S. Faetti, "Infrared refractive indices of liquid crystals," J. Appl. Phys. **97**(7), 073501 (2005).
27. R. Caputo, G. Palermo, M. Infusino, and L. De Sio, "Liquid crystals as an active medium: novel possibilities in plasmonics," Nanospectroscopy **1**(1), 2300–3537 (2015).
28. T. S. Perova, V. A. Tolmachev, E. V. Astrova, Y. A. Zharova, and S. M. O'Neill, "Tunable one-dimensional photonic crystal structures based on grooved Si infiltrated with liquid crystal E7," Phys. Status Solidi C **4**(6), 1961–1965 (2007).
29. A. A. Komar, D. N. Neshev, and A. E. Miroshnichenko, "Tunable dielectric metasurfaces based on the variation of the refractive index of the environment," JETP Lett. **106**(11), 709–715 (2017).
30. P. Grahn, A. Shevchenko, and M. Kaivola, "Electromagnetic multipole theory for optical nanomaterials," New J. Phys. **14**(9), 093033 (2012).

Optics EXPRESS

31. H. W. Kim, J. H. Mun, C. S. Yoon, and J. D. Kim, "Second harmonic generation and photorefractive effect in dye-doped liquid crystals," Jpn. J. Appl. Phys. **40**(Part 2, No. 9A/B), L952–L954 (2001).
32. D. Rocco, M. A. Vincenti, and C. De Angelis, "Boosting Second Harmonic Radiation from AlGaAs Nanoantennas with Epsilon-Near-Zero Materials," Appl. Sci. **8**(11), 2212 (2018).
33. L. Ghirardini, G. Marino, V. F. Gili, I. Favero, D. Rocco, L. Carletti, A. Locatelli, C. De Angelis, M. Finazzi, M. Celebrano, D. N. Neshev, and G. Leo, "Shaping the nonlinear emission pattern of a dielectric nanoantenna by integrated holographic gratings," Nano Lett. **18**(11), 6750–6755 (2018).